Dispersion of the second-order nonlinear susceptibility in ZnTe, ZnSe, and ZnS

H. P. Wagner and M. Kühnelt
Institut Physik II, Universität Regensburg, D-93040 Regensburg, Germany

W. Langbein and J. M. Hvam
Mikroelektronik Centret, The Technical University of Denmark, Building 345 e, 2800 Lyngby, Denmark
(Received 13 March 1998)

We have measured the absolute values of the second-harmonic generation (SHG) coefficient $|d|$ for the zinc-blende II-VI semiconductors ZnTe, ZnSe, and ZnS at room temperature. The investigated spectral region of the fundamental radiation λ_F ranges from 520 to 1321 nm using various pulsed laser sources. In the transparent region of the II-VI semiconductors, the SHG coefficient exceeds the values of birefringent materials as ammonium dihydrogen phosphate (ADP) and potassium dihydrogen phosphate (KDP) by one or two orders of magnitudes. Above the E_0 band gap a strong dispersion of $|d|$ is observed, showing a maximum for a second-harmonic frequency close to the E_1 gap. The experimental results are compared to calculated values using a simple three-band model including spin-orbit splitting. Substantial agreement is found to the experimentally observed dispersion of the second-order nonlinear susceptibility. [S0163-1829(98)06539-4]

I. INTRODUCTION

Experiments on second-harmonic generation (SHG) in II-VI semiconductors date back to the year 1963. Using a Nd:YAG laser (where YAG denotes yttrium aluminum garnet) Miller, Kleinmann, and Savage[1] determined the second-order nonlinear coefficient $|\chi_{14}^{(2)}|$ of CdS, which was found to be 60 times higher than in potassium dihydrogen phosphate (KDP). Subsequent investigations on other II-VI crystals[2–8] confirmed the observation of high second-harmonic generation coefficients, but were mostly restricted to the fundamental wavelengths of $\lambda_F = 1.06\ \mu$m (Nd:YAG laser) and $\lambda_F = 10.6\ \mu$m (CO_2 laser) due to the lack of tunable high-intensity laser sources. Experiments on the dispersion of the second-order nonlinear susceptibility in ZnTe, InSb, GaAs, and InAs were carried out by Chang, Dukuing, and Blombergen[9] using nine discrete fundamental radiation sources. With the advent of dye lasers, more systematic experimental results became available,[10–12] mainly acquired from III-V semiconductors. Only few investigations report on the dispersion of $|\chi_{14}^{(2)}|$ in wide-gap II-VI semiconductors,[13,14] although these materials possess high SHG coefficients and thus have the potential for efficient SHG in the visible spectral region using II-VI waveguide structures.[15–17]

A microscopic expression for $|\chi_{14}^{(2)}|$ can be obtained from second-order perturbation calculations.[18–22] However, a complete understanding of the dispersion of $|\chi_{14}^{(2)}|$ requires detailed information of the energies and wave functions of the electronic states in the entire first Brillouin zone (BZ). Therefore, the dispersion of the nonlinear susceptibility can be used as a sensitive test of various band-structure theories, but with the difficulty of measurements of nonlinear properties. The early calculations of $|\chi_{14}^{(2)}|$ in zinc-blende crystals by Bell[23,24] used a simplified three-band model, taking into account the spin-orbit splitting of the valence band at the Γ point. The band structure was modeled around a few principal critical points assuming constant transition matrix elements over the entire BZ. Substantial agreement was found with the experimental results of Chang, Dukuing, and Blombergen.[9] Since then, Fong and Shen[25] have employed pseudopotential band-structure calculations using four conduction and valence bands and Moss and co-workers[26,27] employed an empirical tight-binding calculation of $|\chi_{14}^{(2)}|$ for various III-V and II-VI semiconductors. In general, the agreement with the experiment was improved by these approaches; however, significant differences between theory and available experimental data still exist.

The general interest in the absolute values $|\chi_{14}^{(2)}|$ of wide-gap II-VI semiconductors and the existing discrepancies between the theories and the experimental results prompted us to investigate the dispersion of zinc-blende ZnTe, ZnSe, and ZnS semiconductors in the wavelength range $\lambda_F = 520-1321$ nm of the fundamental radiation. The data obtained are compared to the theory proposed by Bell[23] including the spin-orbit coupling of the valence band.

II. EXPERIMENTAL SETUP

The absolute values of the SHG coefficient in zinc-blende ZnTe, ZnSe, and ZnS bulk crystals were determined using various radiation sources. A diode pumped *Q*-switched Nd:YLF laser (YLF denotes yttrium lithium fluoride) emitting at $\lambda_F = 1.321$ and 1.047 μm was used as the spectrally narrow fundamental light source, having a repetition rate of 1 kHz. The pulse duration measured by a photodiode was $\Delta t = 140$ and 46 ns, respectively, resulting in peak powers of 100 W and 1 kW. In the spectral range of $\lambda_F = 720-1060$ nm a tunable picosecond Ti:sapphire laser with a repetition rate of 82 MHz was employed. Investigations ranging from $\lambda_F = 1050$ to 1210 nm were performed using a potassium titanyl phosphate optical parametric oscillator, which was pumped by the picosecond Ti:sapphire laser. The pulse widths around $\Delta t = 1$ ps were measured by an autocorrelator. The peak power of the near infrared pulses were about 500 W. In the region between $\lambda_F = 520$ and 740

nm, a combination of a regenerative amplified femtosecond Ti:sapphire laser, a white-light generator, and an optical parametric amplifier was used. The pulse widths in this case were adjusted by a pulse shaper to $\Delta t = 200$ fs. The peak power of these pulses was about 20 kW.

The II-VI crystals investigated have been cleaved along the (110) surface to obtain (0.5–3)-mm-thick, plane-parallel bars. The actual length of the samples was determined using a microscope. The fundamental beams were only weakly focused (having a beam waist of approximately $2w_0 = 300\ \mu$m) onto the II-VI samples in order to minimize beam-size effects. The beam diameter at the sample position was determined by a charge coupled device camera. The position of the focus on the (110) cleaving surface was adjusted by moving the sample with a piezoelectric translation stage, which also allows a rotation of the sample perpendicular to the incident beam. The emerging SHG signal went through a polarizer, a color filter, and a quartz-monochromator filter to suppress the fundamental wave. It was detected by a calibrated photon counting system, using a GaAs photomultiplier. All measurements were performed at room temperature.

III. EXPERIMENTAL RESULTS

Wide-gap zinc-blende II-VI semiconductors with symmetry $T_d(43m)$ are optically isotropic, but do not possess a center of inversion. The second-order nonlinear polarization $\mathbf{P}_{2\omega}(t)$ in the adiabatic limit is given by[28]

$$\mathbf{P}_{2\omega}(t)=\varepsilon_0\begin{pmatrix}0&0&0&d&0&0\\0&0&0&0&d&0\\0&0&0&0&0&d\end{pmatrix}\begin{pmatrix}E^2_{\omega,x}(t)\\E^2_{\omega,y}(t)\\E^2_{\omega,z}(t)\\2E_{\omega,y}(t)E_{\omega,z}(t)\\2E_{\omega,z}(t)E_{\omega,x}(t)\\2E_{\omega,x}(t)E_{\omega,y}(t)\end{pmatrix}, \tag{1}$$

where $\mathbf{E}_\omega(t)$ is the electric-field amplitude of the nearly monochromatic fundamental wave $\mathbf{E}_\omega(t)\exp(i\mathbf{k}\cdot\mathbf{r}-i\omega t)$. The subscripts x, y, and z represent the crystal directions (100), (010), and (001). The third-rank SHG tensor elements $d_{14}=d_{25}=d_{36}=d=d(-2\omega;\omega,\omega)$ are related to the elements $\chi^{(2)}(-2\omega;\omega,\omega)$ by $2d=\chi^{(2)}$.

A powerful method to determine the SHG coefficient $|d|$ is the rotating crystal method proposed by Maker *et al.*,[29] which is discussed in detail by Jerphagnon and Kurtz.[30] They derived a relation of the angle dependence of the generated SHG power considering multiple reflections at the crystal boundaries. The emerging second-harmonic power is given by

$$P_{2\omega}(\theta)=\frac{8}{\varepsilon_0 c\pi w_0^2}\,d^2 t_\omega(\theta)^4 T_{2\omega}(\theta)p(\theta)^2 \times\frac{P_\omega^2}{[n(\omega)^2-n(2\omega)^2]^2}\,B(\theta)R(\theta)\sin^2(\psi), \tag{2}$$

with the oscillating term

$$\sin^2(\psi)=\sin^2\left[\frac{2\pi L}{\lambda_F}\left[n(\omega)\cos\,\theta_\omega-n(2\omega)\cos\,\theta_{2\omega}\right]\right] =\sin^2(\Delta\beta L/2). \tag{3}$$

Besides the rotation angle θ (corresponding to θ_ω, $\theta_{2\omega}$ within the crystal) the decisive parameters are the refractive indices $n(\omega)$, the length of the crystal L, the nonlinear coefficient d, the e^{-2} radius of the Gaussian beam waist w_0, the fundamental power P_ω, and the fundamental wavelength λ_F. The angle-dependent transmission factors

$$t_\omega(\theta)=\frac{2\cos\,\theta}{n(\omega)\cos\,\theta+\cos\,\theta_\omega} \tag{4}$$

and

$$T_{2\omega}(\theta)=\frac{2n(2\omega)\cos\,\theta_{2\omega}[\cos\,\theta+n(\omega)\cos\,\theta_\omega][n(\omega)\cos\,\theta_\omega+n(2\omega)\cos\,\theta_{2\omega}]}{[n(2\omega)\cos\,\theta_{2\omega}+\cos\,\theta]^3} \tag{5}$$

of the fundamental and the second-harmonic wave, respectively, are obtained by boundary conditions. The projection factor $p(\theta)=2\cos(\theta_\omega+\pi/4)\cos(\theta_\omega-\pi/4)$ accounts for the tensor character of the nonlinear susceptibility $\overleftrightarrow{\chi}^{(2)}$. $R(\theta)$ and $B(\theta)$ are corrections considering multiple reflections and beam diameter effects as expressed in Ref. 30. The abbreviation $\Delta\beta$ in Eq. (3) is the propagation constant mismatch between the fundamental and the second-harmonic wave.

By varying the incident angle of the Nd:YLF laser beam on the II-VI samples, the intensity of the transmitted second-harmonic wave oscillates due to the interference term [Eq. (3)]. These Maker oscillations of a 1.64-mm-long ZnSe crystal at the fundamental wavelengths of $\lambda_F=1321$ and 1047 nm are shown in Figs. 1(a) and 1(b), respectively. From the angular dependence of the minima the coherence length

$$l_C=\frac{\pi}{\Delta\beta}=\frac{\lambda_F}{4[n(2\omega)-n(\omega)]} \tag{6}$$

can be derived. The coherence length decreases when the E_0 band gap is approached due to the high refractive index dispersion in the II-VI semiconductors and reaches only a few micrometers as summarized in Table I. The accuracy of the measurements is limited by the determination of the sample lengths, which was estimated to $\pm 2\%$.

The absolute value of the SHG coefficient $|d|$ was evaluated from the envelope of the maxima, which was determined according to Eq. (2). The necessary values of the refractive indices were taken from Refs. 31–33 or were calculated from Sellmair equations.[34,35] The shape of the electric field amplitude $\mathbf{E}_\omega(t)$ was approximated to be rect-

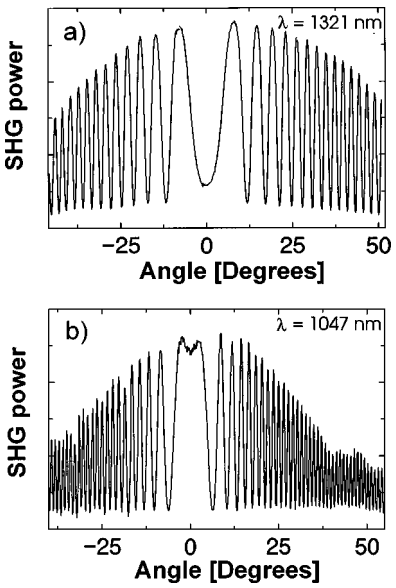

FIG. 1. Maker oscillations as a function of the rotation angle θ obtained from a 1.64-mm-long ZnSe crystal. The fundamental wavelengths are (a) $\lambda_F = 1321$ nm and (b) $\lambda_F = 1047$ nm.

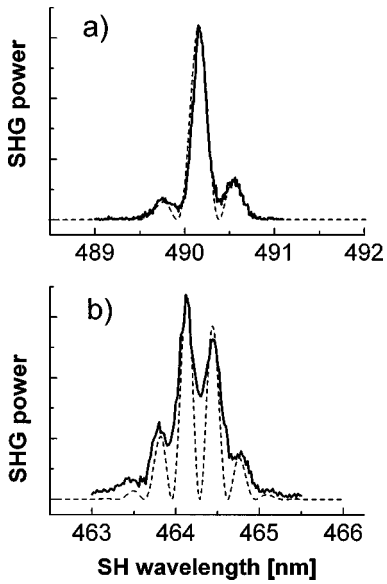

FIG. 2. Second-harmonic power spectrum obtained from a 1.15-mm-long ZnS crystal at normal incidence using the fundamental wavelengths (a) $\lambda_F = 980.4$ nm and (b) $\lambda_F = 928.4$ nm. The pulse widths were $\Delta t = 850$ and 600 fs, respectively. The dotted lines represent the calculated spectra according to Eq. (7).

angular where the peak power is given by $P_\omega = \overline{P}_\omega / r\Delta t$ with average laser power $\overline{P}_\omega$, repetition rate r, and pulse duration Δt. Furthermore, the temporal decrease of the SHG pulse by a factor of approximately $\sqrt{2}$ was taken into account. In addition, finite beam width effects and multiple reflection corrections were considered as treated in Ref. 30. The evaluated $|d|$ values obtained with the pulsed Nd:YLF laser are summarized in Table I and are plotted as full squares in Figs. 3–6. A comparison with absolute values measured by other groups ($\lambda_F = 1.06\ \mu$m) shows good agreement for ZnSe (Ref. 3) and ZnTe.[9]

When a spectrally broad picosecond pulse ($\Delta\lambda \approx 2$ nm) is used, interference effects occur in the spectrum of the SHG signal at normal incidence. Figures 2(a) and 2(b) show this feature at the fundamental wavelengths of $\lambda_F = 980.4$ and 928.4 nm for a ZnS crystal of 1.15 mm length. The temporal pulse widths were $\Delta t = 850$ and 600 fs, respectively. The dashed lines in Fig. 2 are obtained by solving Eq. (2) in the frequency domain according to

$$P_{\omega_2} \approx \frac{C(\omega_0)}{4\gamma} \left| \int_{\omega_2/2}^{\infty} g(\omega_1 - \omega_0) g(\omega_2 - \omega_1 - \omega_0) \times (1 - \gamma e^{i\Delta\beta' L}) d\omega_1 \right|^2 . \quad (7)$$

The function $g(\omega - \omega_0)$ is the Fourier-transformed function of the temporal pulse shape $f(t)$. The used laser system provides Fourier-limited sech(t) field pulses; ω_0 gives the center wavelength of the fundamental pulse. The constant $C(\omega_0)$ contains all factors appearing in Eq. (2) at an angle of $\theta = 0°$ without the oscillating term $\sin^2(\psi)$. γ is given by the relation

$$\gamma = \{2n_{2\omega_0}(n_{\omega_0}+1)\}/\{(n_{2\omega_0}+n_{\omega_0})(n_{2\omega_0}+1)\}. \quad (8)$$

The phase mismatch $\Delta\beta'$ reads

$$\Delta\beta' = \frac{\omega_2 n(\omega_2)}{c} - \frac{\omega_1 n(\omega_1)}{c} - \frac{(\omega_2 - \omega_1) n(\omega_2 - \omega_1)}{c}. \quad (9)$$

Equation (7) accounts for all possible combinations of fundamental frequencies leading to a second-harmonic power at frequency ω_2 around $2\omega_0$ (sum-frequency generation). The theoretically obtained second-harmonic spectrum in Fig. 2 shows good agreement with the experimentally observed data. The lower modulation in the experimental curves is attributed to the limited experimental resolution $\delta\lambda = 0.2$ nm.

TABLE I. Coherence length l_c and SHG coefficients $|d|$ at two fundamental wavelengths provided by the Nd:YLF laser. In addition, values at $\lambda_F = 1.06\ \mu$m obtained from other groups are given.

		$\lambda_F = 1321$ nm		$\lambda_F = 1047$ nm		$\lambda_F = 1.06\ \mu$m
Semiconductor	L (mm)	l_c (μm)	d (pm/V)	l_c (μm)	d (pm/V)	d (pm/V)
ZnTe	1.57	1.62	52		119	90[a]
ZnSe	1.64	2.92	30	1.19	43	27[b]
ZnS	2.54	5.08	8	2.31	12	20[b]

[a]Reference 9.
[b]Reference 3.

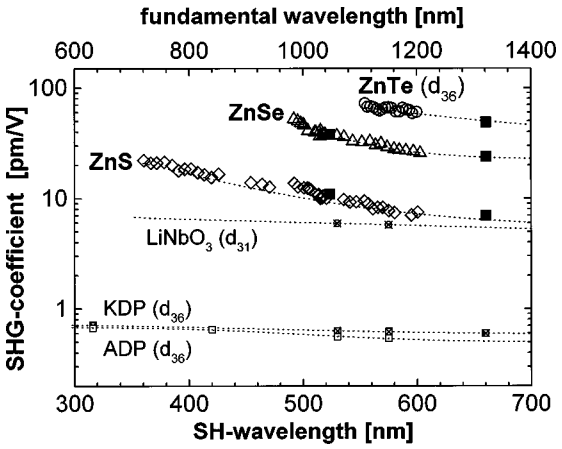

FIG. 3. Dispersion of the SHG coefficient $|d|$ of zinc-blende ZnTe, ZnSe, and ZnS crystals in their second-harmonic transparent spectral region. The black squares represent values obtained with the Nd:YAG laser source. In addition, values of common birefringent materials are shown. The dotted curves are guides for the eye.

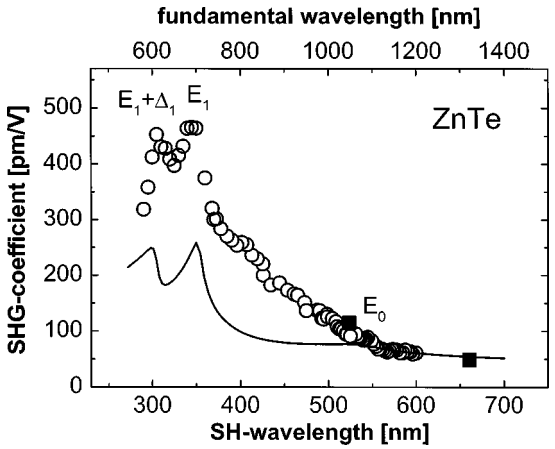

FIG. 4. Experimentally observed dispersion of the SHG coefficient $|d|$ in ZnTe as a function of the fundamental wavelength ranging from $\lambda_F = 570$ to 1321 nm. The black squares represent values obtained with the Nd:YAG laser source. The full line gives the calculated dispersion curve derived with the three-band model [Eq. (12)].

In order to determine the absolute values of the SHG coefficient $|d|$ using picosecond pulses the experiments were performed without spectral resolution. Since we integrate over all Maker oscillations of the second-harmonic power, the measured power was corrected by a factor of 2 to obtain the value of $|d|$ from Eq. (2). (The factor of 2 is valid if more than two oscillations occur in the second-harmonic power spectrum, which was generally the case in the performed experiments.) Again, the shortening of the SHG pulse by a factor of approximately $\sqrt{2}$ was taken into account. In order to minimize the pulse broadening due to the refractive index dispersion of the II-VI crystals, we used pulse widths of about $\Delta t = 1$ ps. The dispersion of the SHG coefficient $|d|$ obtained in the transparent region of the investigated wide gap (II-VI) semiconductors is given in Fig. 3 together with values of some birefringent materials such as ADP,[36] KDP,[37] and $LiNbO_3$,[38] which are generally used in phase-matchable SHG devices. The comparison shows that the SHG coefficients of II-VI semiconductors exceed the values of d_{31} and d_{36} of the birefringent materials by one or two orders of magnitude, indicating II-VI materials as promising materials for efficient second-harmonic generation in the visible spectral range.

When the frequency of the SHG wave exceeds the E_0 band-gap energy, the Maker oscillations disappear due to the strong linear absorption of the second-harmonic wave. The absolute value of the SHG coefficient is now determined using the complex modulus $\tilde{n}(\omega) = n(\omega) + i\kappa(\omega)$. In the case of a strong absorption of the second-harmonic wave [$\alpha(2\omega) \approx 10^5$ cm^{-1}], but weak absorption of the fundamental beam $\kappa(\omega) \approx 0$, the second-harmonic power emitted at normal incidence ($\theta = 0°$) reads[7]

$$P_{2\omega}(\theta = 0°) = \frac{2}{\varepsilon_0 c \pi w_0^2} d^2 t_\omega^4 \times \frac{P_\omega^2}{(\Delta n)^2 + \left(\frac{\lambda_F \alpha(2\omega)}{8\pi}\right)^2} \frac{1}{|\tilde{n}(2\omega) + 1|^2}, \tag{10}$$

with $\alpha(2\omega) = (4\pi/\lambda)\kappa(2\omega)$ and $\Delta n = n(2\omega) - n(\omega)$. Multiple reflections and beam size effects have been neglected. The values of the linear absorption $\alpha(2\omega)$ were taken from the literature.[31–33]

The linear absorption of the second-harmonic wave and the two-photon absorption lead to band-to-band transitions and impurity transitions. The detection of this erroneous radiation is minimized by direction filtering along the wave vector $\mathbf{k}_{2\omega}$ of the SHG beam and by spectral discrimination ($\Delta\lambda \approx 5$ nm) of the SHG light. Within the spectral region from $\lambda_F = 520$ to 740 nm, the pulses possess a temporal width of $\Delta t = 200$ fs. In this case the samples were cut to a length of approximately 0.7 mm in order to avoid a significant pulse broadening of the fundamental wave within the material.

The continuation of the dispersion of the SHG coefficients $|d|$ into the 2ω absorptive regions of the semiconductors ZnTe, ZnSe, and ZnS is shown in Figs. 4, 5, and 6, respectively. In all II-VI semiconductors, an increase of the SHG coefficient is observed when the SHG frequency approaches the E_0 band-gap energy. In the excitonic region of ZnTe only a weak resonance appears. Above the E_0 band gap a strong increase of the SHG coefficient is observed, which is in agreement with the investigation of Chang, Dukuing, and Blombergen.[9] (The absolute values of the nonlinear coefficient $|d|$ are in agreement within a 20% deviation.) The SHG coefficient shows a maximum at the E_1 gap, as already indicated in Ref. 9, and a further peak when the $E_1 + \Delta_1$ band gap is reached. In the ZnSe and ZnS crystals a distinct resonance appears in the vicinity of the E_0 gap. Due to the high exciton binding energies of 20 and 35 meV in ZnSe and ZnS, respectively, the influence of excitonic effects is present at room temperature and the E_0 resonances of $|d|$ are attributed to an excitonic enhancement.

IV. COMPARISON WITH THEORY

The microscopic expression of $\chi^{(2)}_{xyz}$ obtained from second-order perturbation calculations[18–22] is given by

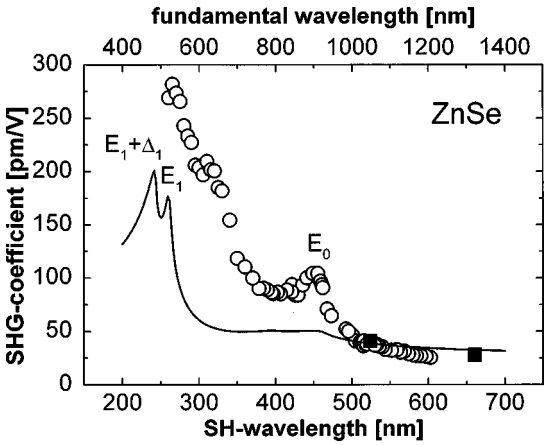

FIG. 5. Experimentally observed dispersion of the SHG coefficient $|d|$ in ZnSe as a function of the fundamental wavelength λ_F ranging from 520 to 1321 nm. The black squares represent values obtained with the Nd:YAG laser source. The full line gives the calculated dispersion curve [Eq. (12)].

$$\chi^{(2)}_{\mu\alpha\beta}(-2\omega,\omega,\omega) = -i\,\frac{1}{32\varepsilon_0}\left(\frac{e}{m_0\pi\omega}\right)^3 \sum_{n,n',n''}\int_{\mathrm{BZ}} d^3\mathbf{k} \times f_{n\mathbf{k}}\left\{\frac{p^{\mu}_{nn'}p^{\alpha}_{n'n''}p^{\beta}_{n''n}+p^{\mu}_{nn'}p^{\beta}_{n'n''}p^{\alpha}_{n''n}}{[E_{n'n}(\mathbf{k})-2\hbar\omega][E_{n''n}(\mathbf{k})-\hbar\omega]} + \frac{p^{\alpha}_{nn'}p^{\mu}_{n'n''}p^{\beta}_{n''n}+p^{\beta}_{nn'}p^{\mu}_{n'n''}p^{\alpha}_{n''n}}{[E_{n'n}(\mathbf{k})+\hbar\omega][E_{n''n}(\mathbf{k})-\hbar\omega]} + \frac{p^{\beta}_{nn'}p^{\alpha}_{n'n''}p^{\mu}_{n''n}+p^{\alpha}_{nn'}p^{\beta}_{n'n''}p^{\mu}_{n''n}}{[E_{n'n}(\mathbf{k})+\hbar\omega][E_{n''n}(\mathbf{k})+2\hbar\omega]}\right\}, \quad \mu,\alpha,\beta\in\{x,y,z\}. \tag{11}$$

Here the electrons are assumed to occupy Bloch states $\psi_{n,\mathbf{k}}(\mathbf{r})=u_{n,\mathbf{k}}(\mathbf{r})\exp(i\mathbf{k}\cdot\mathbf{r})$ specified by the band label n and wave vector $\mathbf{k}$ with the energy $E_n(\mathbf{k})$. $f_{n,\mathbf{k}}$ is the equilibrium Fermi-Dirac occupation function for the state $\psi_{n,\mathbf{k}}(\mathbf{r})$ and $\mathbf{p}_{n,n'}(\mathbf{k})$ is the matrix element of the linear momentum operator between states $\psi_{n,\mathbf{k}}(\mathbf{r})$ and $\psi_{n',\mathbf{k}}(\mathbf{r})$. $E_{n'n}(\mathbf{k})$ is the corresponding transition energy $E_{n'}(\mathbf{k})-E_n(\mathbf{k})$.

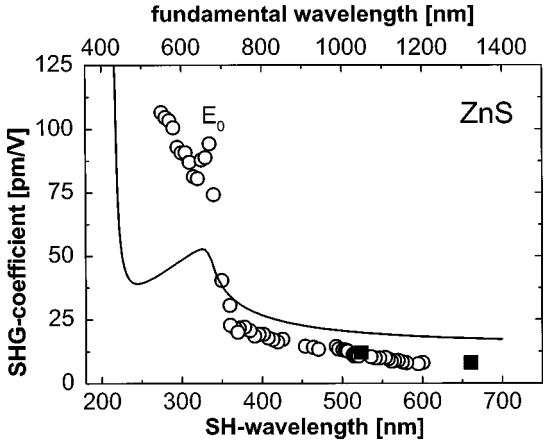

FIG. 6. Experimentally observed dispersion of the SHG coefficient $|d|$ in ZnS as a function of the fundamental wavelength λ_F ranging from 520 to 1321 nm. The black squares represent values obtained with the Nd:YAG laser source. The full line gives the calculated dispersion curve [Eq. (12)].

At least three bands are necessary to obtain a contribution to $\chi^{(2)}_{xyz}$,[23,24,39] since if only two bands are considered, the contributions for $\mathbf{k}$ and $-\mathbf{k}$ cancel each other. Neglecting spin-orbit coupling, the top valence band Γ_{15v} and the two lowest conduction bands (Γ_1,Γ_{15c}) constitute a minimal set of three bands with a finite contribution to $\chi^{(2)}_{xyz}$. Even with these simplifications, Eq. (11) is not amenable without a detailed information of the energies and the wave functions of the electronic states in the first BZ. To avoid extensive full band-structure calculations, we follow the approach of Bell,[23] modelling the bands around a few principal critical points. Such points exist at the Γ point $\mathbf{k}=\mathbf{0}$ (the E_0,E_0' gap), and along $\mathbf{k}=(k/\sqrt{3})(111)$ approaching the L points (the E_1,E_1' gap). The X points (the E_2 gap) were neglected here due to the large E_2 energy.

The E_0,E_0' transitions are represented by three-dimensional parabolic bands extending to infinite $\mathbf{k}$, yielding the expression

$$\chi^{(2)}_{xyz}(-2\omega,\omega,\omega)=C_\Gamma(PP'Q)\,\frac{1}{\omega^3}\,\frac{1}{\alpha_1\alpha_2}\sum_1^6 S_iT_i(x_i,x_i'), \tag{12}$$

with

$$C_\Gamma=-i\,\frac{1}{4\pi\varepsilon_0}\left(\frac{e}{\hbar}\right)^3,\quad x_i=\frac{E_0+\nu_i\hbar\omega}{\alpha_1},$$

$$x_i'=\frac{E_0'+\mu_i\hbar\omega}{\alpha_2},\quad T_i(x_i,x_i')=\frac{1}{\sqrt{x_i}+\sqrt{x_i'}},$$

$$S_i=\begin{cases}1, & i=1,2,3\\ -1, & i=4,5,6\end{cases}$$

$$\nu_i=-2,+1,+1,-1,-1,+2,$$

$$\mu_i=-1,-1,+2,-2,+1,+1.$$

$\alpha_1=\hbar^2/2m_{vc}$ and $\alpha_2=\hbar^2/2m_{vc'}$ represent the inverse reduced masses of a band pair. We assume that the products of the three matrix elements of the linear momentum operator $PP'Q$ between the p-like Γ_{15v} valence band and the s-like Γ_1 conduction band $(P=\hbar/m_0\int_\Omega\psi^t_{cS}p_x\psi_{vX}d^3x)$, between the Γ_1 conduction band and p-like Γ_{15c} conduction band $(P'=\hbar/m_0\int_\Omega\psi^t_{cS}p_x\psi_{c'X}d^3x)$, and between the Γ_{15v} valence band and Γ_{15c} conduction band $(Q=\hbar/m_0\int_\Omega\psi^t_{vX}p_y\psi_{c'Z}d^3x)$ remain constant over the entire BZ.

The E_1,E_1' transitions are represented by two-dimensional parabolic bands. [The effective masses along the (111) direction are assumed to be infinity due to the nearly parallel conduction and valence bands.] Integration over the BZ yields an expression of the form of Eq. (12) with

$$C_L=-i\,\frac{\sqrt{3}}{\varepsilon_0 a_0\pi}\left(\frac{e}{\hbar}\right)^3,\quad x_i=\frac{E_1+\nu_i\hbar\omega}{\alpha_1'},$$

TABLE II. Parameters used for calculating the dispersion of the SHG coefficient $|d|$ according to Eq. (12).

Parameter	ZnTe	ZnSe	ZnS
E_0 (eV)	2.28[a]	2.69[b]	3.68[j]
E_0' (eV)	5.4[b]	8.45[f]	5.79[k]
Δ_0 (eV)	0.92[a]	0.4[b]	0.07[j]
E_1 (eV)	3.52[c]	4.75[g]	5.73[j]
E_1' (eV)	6.9[c]	9.1[g]	9.78[k]
Δ_1 (eV)	0.56[c]	0.35[g]	
m_e^* (m_0)	0.122[d]	0.145[h]	0.22[h]
γ_1	3.8[d]	2.45[i]	2.54[l]
γ_2	0.72[d]	0.61[i]	0.75[l]
γ_3	1.3[d]	1.11[i]	1.09[l]
P (eV nm)	0.89	0.85	1.02
P'/i (eV nm)	0.35	0.44	0.55
Q (eV nm)	0.74	0.72	0.6
a_0 (nm)	6.1035[e]	5.6687[e]	5.4102[m]

[a]Reference 31.
[b]Reference 45.
[c]Reference 46.
[d]Reference 47.
[e]Reference 48.
[f]Reference 49.
[g]Reference 50.
[h]Reference 51.
[i]Reference 52.
[j]Reference 53.
[k]Reference 54.
[l]Reference 55.
[m]Reference 56.

$$x_i'=\frac{E_1'+\mu_i\hbar\omega}{\alpha_2'},\quad T_i(x_i,x_i')=\frac{1}{x_i-x_i'}\ln\left(\frac{x_i}{x_i'}\right).$$

The inverse effective masses α_1 and α_2 have to be replaced by the inverse reduced masses α_1' and α_2' in the vicinity of the L points. The S_i, ν_i, and μ_i are defined as in Eq. (12) and a_0 is the lattice constant.

The calculated values of the SHG coefficient $|d|$ are shown in Figs. 4–6 as full lines for the ZnTe, ZnSe, and ZnS crystals, respectively. Thereby the spin-orbit splitting of the Γ_{15v} valence band was taken into account, whereas the spin-orbit splitting of the Γ_{15c} conduction band has been neglected. The material parameters used in the calculation are summarized in Table II. The transition matrix elements P,P',Q were evaluated according to $\mathbf{k}\cdot\mathbf{p}$ perturbation theory by[40–43]

$$Q=\frac{\hbar}{m_0}\sqrt{\frac{m_0E_0'}{2}\left(\frac{m_0}{m_{\rm hh}}+1\right)}, \tag{13}$$

$$P=\frac{\hbar}{m_0}\sqrt{\left(\frac{m_0}{m_{\rm lh}}+1-\frac{2(Qm_0/\hbar)^2}{3m_0E_0'}\right)\frac{3m_0E_0}{4}}, \tag{14}$$

$$P'=i\,\frac{\hbar}{m_0}\left\{-\left[\frac{m_0}{m_e^*}-1-\frac{2(Pm_0/\hbar)^2}{3m_0}\times\left(\frac{2}{E_0}+\frac{1}{E_0+\Delta_0}\right)\right]\frac{m_0(E_0'-E_0)}{2}\right\}^{1/2}, \tag{15}$$

using the observed effective electron masses m_e^* and the spherical part of the heavy-hole $m_{\rm hh}$ and light-hole $m_{\rm lh}$ masses given by[44]

$$m_{\rm hh,(lh)}=\frac{m_0}{\gamma_1}\left(1-(+)\,\frac{6\gamma_3+4\gamma_2}{5\gamma_1}\right)^{-1}, \tag{16}$$

where m_0 is the vacuum electron mass and γ_1, γ_2, and γ_3 are the Luttinger parameters.

The effective masses of the spin-orbit split-off Γ_7 valence band $m_{\rm so}$ as well as the reduced effective masses α_1' and $\alpha_{1\Delta_1}'$ between the spin-orbit split L_{3v} valence bands $(L_{4,5},L_6)$ and the L_{1c} conduction band, respectively, were calculated according to the relations[40,42]

$$\frac{m_0}{m_{\rm so}}=-1+\frac{2(Pm_0/\hbar)^2}{3m_0(E_0+\Delta_0)}+\frac{4(Qm_0/\hbar)^2}{3m_0(E_0'+\Delta_0)} \tag{17}$$

and

$$\alpha_1'=P^2\left(\frac{1}{E_1}+\frac{1}{2(E_1+\Delta_1)}\right), \tag{18}$$

$$\alpha_{1\Delta_1}'=P^2\left(\frac{1}{2E_1}+\frac{1}{E_1+\Delta_1}\right). \tag{19}$$

The effective mass of the Γ_{15c} conduction band was approximated by the mean hole mass $m_h=m_0/\gamma_1$. The inverse reduced mass α_2' between the L_{3c} conduction band, where spin-orbit coupling has been neglected, and the split L_{3v} $(L_{4,5},L_6)$ valence bands were assumed to be $\alpha_2'=\hbar^2/m_h$. As proposed in Ref. 23, the transition energies were thermally broadened by an energy of $\eta=0.03$ eV ($\approx k_BT$) for the sake of comparison with observations at room temperature.

The measured absolute values and the dispersion of the SHG coefficient $|d|$ are reproduced within a factor of 2 for the investigated II-VI crystals. In all materials, a resonant enhancement is observed at the corresponding E_0 gap energy. Above the E_0 gap the growing influence of the L points becomes important, which explains the strong increase of the SHG coefficient in ZnTe and ZnSe close to the E_1 gap. Furthermore the structure caused by the $E_1+\Delta_1$ band gap is reproduced in the ZnTe crystal. Relatively strong deviations, however, occur in the energy range between the Γ point and the L points where the model underestimates the experimentally observed dispersion of $|d|$.

V. DISCUSSION

The experimental accuracy in the determination of the SHG coefficients $|d|$ is mainly limited by the calibration of the detection system and by the determination of the beam diameter within the sample. Both uncertainties lead to an total experimental error of $\pm 20\%$. However, since we do not use a nonlinear standard as other groups,[9–14] but a calibrated GaAs photomultiplier, the experimental error does not affect the dispersive structure of $|d|$, but only changes its absolute value. The uncertainty of the refractive index values and the linear absorption does not lead to a significant error (smaller than $\pm 5\%$). The influence of laser fluctuations on the accuracy ($<5\%$ peak to peak) is also not important. Sample heating caused by the laser pulses is estimated to be insignificant as the used pulse energies are in the order of a few nanojoules. Since a spectral discrimination was used in our experiments, the influence of erroneous impurity or band-to-

band luminescence was also negligible.

The existing discrepancies between the theoretical modelling and the experimental data are thus attributed to inaccuracies of the model. One weak point of the applied model is the use of only one valence band and two conduction bands while other bands are neglected. Furthermore, transitions along the Δ direction have been neglected and effective masses are used, which are roughly estimated at the L points. On the other hand, the discrepancies still exist if a full band-structure calculation using an empirical tight-binding method is applied.[27] Again, a minimum of d occurs above the E_0 gap that is in contrast to the experimental data. Since these calculations neglect the spin-orbit interaction of the valence band, the agreement with the experimentally observed structure of $|d|$ is even weaker than that obtained with the simplified model by Bell. A significant improvement is expected, however, if more than three bands are considered as has been shown by Fong and Shen calculating $|d|$ of various III-V semiconductors.[25] Using an empirical pseudopotential method that includes the spin-orbit coupling of essential bands, a better reproduction of the experiments is found. In particular, the saddle point above the E_0 gap is much less pronounced in the calculated curves. Furthermore, the discrepancies between theory and experiment are attributed to the neglect of the Coulomb interaction between the electron and hole, which influences strongly not only the dispersion at the E_0 gap but also for higher transitions. Since the dispersion of the SHG coefficient $|d|$ can be regarded as a more sensitive test to band structure theories than the linear dielectric constant $\varepsilon(\omega)$, the acquired nonlinear data thus provoke repeated calculations with improved theoretical models including also excitonic effects.

VI. SUMMARY

We have performed precise measurements of the SHG coefficient $|d|$ in ZnTe, ZnSe, and ZnS crystals within the spectral region between $\lambda_F = 520$ and 1321 nm. Our results in ZnTe agree with earlier measurements of Chang, Dukuing, and Blombergen.[9] The structure of the dispersion of $|d|$ can clearly be interpreted as two-photon resonances derived from a three-band model considering the spin-orbit splitting of the valence band. The model reproduces the absolute values in the transparent region of the II-VI materials within a factor of 2. Furthermore, the structure of $|d|$ is correctly reproduced in the vicinity of the L points. However, significant discrepancies occur in the energy range between the E_0 gap and the E_1 gap. The deviations between theory and experimental results are attributed to the simplified consideration of only one valence band and two top conduction bands and to the neglect of the Coulomb interaction between the electron and hole.

ACKNOWLEDGMENTS

The experimental support of H. Schmitzer and S. Wittmann is kindly acknowledged. This work was supported by the Deutsche Forschungsgemeinschaft, Deutsche Telekom, and the Danish Ministries of Research and Industry in the framework of CNAST.

[1] R. C. Miller, D. A. Kleinmann, and A. Savage, Phys. Lett. **11**, 146 (1963).
[2] C. K. N. Patel, Phys. Rev. Lett. **16**, 613 (1966).
[3] R. A. Soref and H. W. Moss, J. Appl. Phys. **35**, 2152 (1964).
[4] G. D. Boyd, E. Buehler, and F. G. Storz, Appl. Phys. Lett. **18**, 301 (1971).
[5] R. L. Herbst and R. L. Byer, Appl. Phys. Lett. **19**, 527 (1971).
[6] M. M. Choy and R. L. Byer, Phys. Rev. B **14**, 1693 (1976).
[7] R. C. Miller and W. A. Nordland, Phys. Rev. B **2**, 4896 (1970).
[8] R. C. Miller and W. A. Nordland, Opt. Commun. **1**, 400 (1970).
[9] R. K. Chang, J. Dukuing, and N. Blombergen, Phys. Rev. Lett. **15**, 415 (1965).
[10] H. Lotem, G. Koren, and V. Yacoby, Phys. Rev. B **9**, 3532 (1974).
[11] F. G. Parsons and R. K. Chang, Opt. Commun. **3**, 173 (1971).
[12] D. Bethune, A. J. Schmidt, and Y. R. Shen, Phys. Rev. B **11**, 3867 (1975).
[13] F. G. Parsons, E. Yi Cen, and R. K. Chang, Phys. Rev. Lett. **27**, 1436 (1971).
[14] M. S. Yeganeh, J. P. Culver, A. G. Yodh, and M. C. Tamargo, Phys. Rev. B **46**, 1603 (1992).
[15] H. P. Wagner, S. Wittmann, H. Schmitzer, and H. Stanzl, J. Appl. Phys. **77**, 3637 (1995).
[16] H. P. Wagner, M. Kühnelt, G. Wein, W. Gebhardt, D. Eisert, G. Bacher, and A. Forchel, J. Lumin. **72-74**, 87 (1997).
[17] M. Kühnelt, T. Leichtner, S. Kaiser, B. Hahn, H. P. Wagner, D. Eisert, G. Bacher, and A. Forchel, Appl. Phys. Lett. **73**, 584 (1998).
[18] J. A. Armstrong, N. Bloembergen, J. Duking, and P. S. Pershan, Phys. Rev. **127**, 1918 (1962).
[19] P. N. Butcher and T. P. McLean, Proc. Phys. Soc. London **81**, 219 (1963).
[20] P. N. Butcher and T. P. McLean, Proc. Phys. Soc. London **83**, 579 (1964).
[21] P. L. Kelley, J. Phys. Chem. Solids **24**, 607 (1963).
[22] P. L. Kelley, J. Phys. Chem. Solids **24**, 1113 (1963).
[23] M. I. Bell, in *Electronic Density of States*, edited by L. H. Bennet, Natl. Bur. Std. (U.S.), Spec. Publ. No. 323 (U.S. GPO, Washington, DC, 1971), p. 757.
[24] M. I. Bell, Phys. Rev. B **6**, 516 (1972).
[25] C. Y. Fong and Y. R. Shen, Phys. Rev. B **12**, 2325 (1975).
[26] D. J. Moss, J. E. Sipe, and H. M. van Driel, Phys. Rev. B **36**, 9708 (1987).
[27] E. Ghahrramani, D. J. Moss, and J. E. Sipe, Phys. Rev. B **43**, 9700 (1991).
[28] See, for example, P. N. Butcher and D. Cotter, *The Elements of Nonlinear Optics*, Cambridge Studies in Modern Physics Vol. 9 (Cambridge University Press, Cambridge, 1990).
[29] P. D. Maker, R. W. Terhune, M. Nisenoff, and C. M. Savage, Phys. Rev. Lett. **8**, 21 (1962).
[30] J. Jerphagnon and S. K. Kurtz, J. Appl. Phys. **41**, 1667 (1970).
[31] K. Sato and S. Adachi, J. Appl. Phys. **73**, 926 (1993).
[32] S. Adachi and T. Taguchi, Phys. Rev. B **43**, 9569 (1991).
[33] S. Ozaki and S. Adachi, Jpn. J. Appl. Phys., Part 1 **32**, 5008 (1993).

[34] L. Ward, in *Handbook of Optical Constants of Solids II*, edited by E. D. Palik (Academic, Boston, 1991), p. 737.
[35] D. T. F. Marple, J. Appl. Phys. **35**, 539 (1964).
[36] *Tables of Physical Constants*, edited by I. K. Kikoin (Atomizdat, Moscow, 1976).
[37] M. M. Choy and R. L. Byer, Phys. Rev. B **14**, 1693 (1976).
[38] J. Jerphagnon, S. K. Kurtz, and J. L. Oudar, in *Crystal and Solid State Physics*, Landolt Börnstein, New Series, Group 3, Vol. 18, Pt. a (Springer, Berlin, 1984), p. 456.
[39] M. Cardona and F. H. Pollak, in *The Physics of Optoelectronic Materials*, edited by W. A. Albers, Jr. (Plenum, New York, 1971), p. 81.
[40] P. Yu and M. Cardona, *Fundamentals of Semiconductors* (Springer, Berlin, 1996).
[41] M. Cardona, J. Phys. Chem. Solids **24**, 1543 (1963).
[42] M. Cardona, in *Atomic Structure and Properties of Solids*, Proceedings of the International School of Physics ''Enrico Fermi,'' Course LII, Varenna, 1972, edited by E. Burnstein (Academic, New York, 1972).
[43] C. Hermann and C. Weisbuch, Phys. Rev. B **15**, 823 (1977).
[44] A. Baldereschi and N. O. Lipari, Phys. Rev. B **8**, 2697 (1973).
[45] E. Matatagui, A. G. Thompson, and M. Cardona, Phys. Rev. **176**, 950 (1968).
[46] M. Cardona and D. L. Greenaway, Phys. Rev. **131**, 98 (1963).
[47] H. P. Wagner, S. Lankes, K. Wolf, D. Lichtenberger, W. Kuhn, P. Link, and W. Gebhardt, J. Lumin. **52**, 41 (1992).
[48] W. L. Roth, in *Physics and Chemistry of II-VI Compounds*, edited by M. Aven and J. S. Penner (North-Holland, Amsterdam, 1967), p. 119.
[49] F. H. Pollak, in *II-VI Semiconducting Compounds*, edited by D. G. Thomas (Benjamin, New York, 1967), p. 552.
[50] D. L. Greenaway and G. Harbeke, in *Optical Properties and Band Structure of Semiconductors* (Pergamon, Oxford, 1968).
[51] N. Miura, Y. Imanaka, and H. Nojiri, Mater. Sci. Forum **182-184**, 287 (1995).
[52] H. W. Hölscher, A. Nöthe, and Ch. Vihlein, Phys. Rev. B **31**, 2379 (1985).
[53] D. Theis, Phys. Status Solidi B **79**, 125 (1977).
[54] M. Cardona and G. Harbeke, Phys. Rev. A **137**, 1467 (1965).
[55] P. Lawaetz, Phys. Rev. B **4**, 3460 (1971).
[56] R. R. Reeber, Phys. Status Solidi A **32**, 321 (1975).